the plant journal

SEB SOCIETY FOR EXPERIMENTAL BIOLOGY

The Plant Journal (2024) **120**, 2683–2699 doi: 10.1111/tpj.17138

A multiomics investigation into the evolution and specialized metabolisms of three *Toxicodendron* cultivars

Dan Zong[1,‡], Yan Xu[2,‡], Xiaolin Zhang[1,‡], Peihua Gan[1,‡], Hongli Wang[2], Xiayi Chen[2], Hongping Liang[2], Jintao Zhou[1], Yu Lu[1], Peiling Li[1], Shaojie Ma[1], Jinde Yu[1], Tao Jiang[1], Shengxi Liao[3], Meirong Ren[1], Linzhou Li[2,4], Huan Liu[4], Sunil Kumar Sahu[2,4,*], Laigeng Li[5,*], Sibo Wang[2,4,*] and Chengzhong He[1,*,†]

[1]*Key Laboratory for Forest Genetic and Tree Improvement and Propagation in Universities of Yunnan Province, Southwest Forestry University, Kunming 650224, China,*
[2]*BGI Research, Wuhan 430074, China,*
[3]*Institute of Highland Forest Science, Chinese Academy of Forestry, Kunming 650216, China,*
[4]*BGI Research, Shenzhen 518083, China, and*
[5]*Key Laboratory of Plant Carbon Capture, CAS Center for Excellence in Molecular Plant Sciences, Chinese Academy of Sciences, Shanghai 20032, China*

Received 27 March 2024; revised 21 October 2024; accepted 28 October 2024; published online 26 November 2024.
*For correspondence (e-mail hecz@swfu.edu.cn; wangsibo1@genomics.cn; lgli@cemps.ac.cn and sunilkumarsahu@genomics.cn).
[†]Deceased.
[‡]These authors contributed equally to this work.

SUMMARY

Toxicodendron **species are economically and medicinally important trees because of their rich sources of natural products. We present three chromosome-level genome assemblies of *Toxicodendron vernicifluum* 'Dali', *Toxicodendron succedaneum* 'Vietnam', and *T. succedaneum* 'Japan', which display diverse production capacities of specialized metabolites. Genome synteny and structural variation analyses revealed large genomic differences between the two species (*T. vernicifluum* and *T. succedaneum*) but fewer differences between the two cultivars within the species. Despite no occurrence of recent whole-genome duplications, *Toxicodendron* showed evidence of local duplications. The genomic modules with high expression of genes encoding metabolic flux regulators and chalcone synthase-like enzymes were identified via multiomics analyses, which may be responsible for the greater urushiol accumulation in *T. vernicifluum* 'Dali' than in other *Toxicodendron* species. In addition, our analyses revealed the regulatory patterns of lipid metabolism in *T. succedaneum* 'Japan', which differ from those of other *Toxicodendron* species and may contribute to its high lipid accumulation. Furthermore, we identified the key regulatory elements of lipid metabolism at each developmental stage, which could aid in molecular breeding to improve the production of urushiol and lipids in *Toxicodendron* species. In summary, this study provides new insights into the genomic underpinnings of the evolution and diversity of specialized metabolic pathways in three *Toxicodendron* cultivars through multiomics studies.**

Keywords: ***Toxicodendron*, urushiol, lipids, natural products, multiomics.**

INTRODUCTION

Toxicodendron (a toxic tree in Greek) is a genus of woody plants in the Anacardiaceae family, comprising ~30 species, such as poison ivy (*Toxicodendron radicans*) and poison sumac (*Toxicodendron vernix*), which are commonly known for their general toxicity caused by an oily allergen called urushiol (Frankel, 1991; Majima, 1922; Majima & Chō, 1907; Nie et al., 2009; Niimura et al., 1996; Qin et al., 1996; Snyder, 1989; Symes & Dawson, 1953; Yamauchi et al., 1980). Urushiol, which can be collected from the sap of *Toxicodendron*, is an oily mixture of 15- and 17-carbon side chain alk-(en)-yl catechols and resorcinols (Dawson & Kurtz, 1971; Geissman, 1963; Sunthankar & Dawson, 1954). Although urushiol causes allergies and contact dermatitis in many individuals, urushiol has attracted attention for its pharmacological properties, such as anticancer, antibacterial, and antioxidant effects, (Cho et al., 2015; Gladman, 2006; Oshima et al., 1985; Saravanakumar et al., 2019; Snyder, 1989; Suk et al., 2011; Sunthankar & Dawson, 1954; Xie et al., 2016; Zhao et al., 2009). Although recent studies have suggested that chalcone synthases, which are involved in flavonoid metabolism within the polyketide synthase (PKS) family, might catalyze a key step in urushiol biosynthesis (Bai et al., 2022; Wang et al., 2020), the complete urushiol biosynthetic pathway remains unclear (Bai et al., 2022). The *PKS* family was also proposed to coordinate with fatty acid (FA) metabolism-related enzymes such as long-chain-fatty-acid-CoA ligase (LCAS) and 3-ketoacyl-CoA synthase (KCS) to convert long-chain FA or FA metabolism intermediates during the formation of urushiol (Bai et al., 2018, 2022; Weisberg, 2014).

Raw lacquer, a potent natural coating, is synthesized primarily in the specialized cells of the phloem tissue in various *Toxicodendron* species (Aziz et al., 2017; Wei et al., 2009; Zhao, 2021); it is known as "the king of coatings" in Asia and possesses great economic value (Li, Li, & Fang, 2022). In addition, their fruits also hold significant economic value and can be used in the production of vegetable waxes and oils (Beaman, 1986; Kamiya et al., 2002; Tsujimoto, 1935). Because lipids contain a variety of necessary FAs with high nutritional value, particularly linoleic acid, comparable to peanut oil and sesame oil, the production of edible oil from *Toxicodendron* fruits has significant promise (Liu et al., 2022). However, the synthesis of specialized natural products in different *Toxicodendron* species varies. For example, *T. vernicifluum* (also known as the Chinese lacquer tree) can produce abundant sap from its wounded phloem, while the most economically important fruit of *T. succedaneum* is its larger lipid-rich fruits, in contrast to the smaller fruits of *T. vernicifluum*. Both *T. vernicifluum* 'Dali' and *T. succedaneum* 'Japan' (also known as the wax tree) are economically important trees in Asia. The former is mainly used to extract raw lacquer, and the latter is often used for wax and oil production. *T. Succedaneum* 'Vietnam' is another commercially important cultivar that is widely distributed in Vietnam and Yunnan Province in China (Yu, 2014). However, the fruit size of *T. succedaneum* 'Vietnam' is relatively smaller than that of the wax tree (Figure 1D). Furthermore, the greater water content and lower urushiol content in its sap result in the quality of the raw lacquer being lower than that of the lacquer tree (Yu, 2014). The underlying mechanism for the differentiated capacity for producing specialized metabolites in different *Toxicodendron* cultivars could be explored based on a multiomics approach, which has been applied to illustrate the evolution and regulation of specific metabolic pathways in plant species, such as *Torreya grandis* (Lou et al., 2023) and *Camellia sinensis* (Zhang et al., 2021).

The genomes of two *Toxicodendron* species (in three cultivars, *T. vernicifluum* 'Dali', *T. succedaneum* 'Vietnam', and *T. succedaneum* 'Japan') were sequenced in this study. These genomes, along with the genome of another cultivar, *T. vernicifluum* 'Gaobachi' (Bai et al., 2022), were used to study how the genomes of different *Toxicodendron* species evolved in these species. Moreover, we used time-ordered comparative multiomics analysis to determine how urushiol and lipids are produced in different species of *Toxicodendron*. Overall, the three high-quality *Toxicodendron* genomes, combined with multiomics analyses, revealed deep insights into the genomic evolution and specialized metabolism of natural products among *Toxicodendron* species, which will aid in molecular breeding for improving urushiol and lipid production in these species.

RESULTS

Genome assembly and annotation

We assembled the genomes of three cultivars of two *Toxicodendron* species, namely, *T. vernicifluum* 'Dali' (TvD), *T. succedaneum* 'Vietnam' (TsV) and *T. succedaneum* 'Japan' (TsJ), by combining short-read, Nanopore long-read, and Hi-C data. The final genome assemblies were 469, 575 and 588 Mb with contig N50 lengths of 18.8, 1.3 and 6.0 Mb for TvD, TsV, and TsJ, respectively (Table S2), which are close to their estimated genome sizes using k-mer distribution analysis (Figure S2). Using Hi-C contact information, the contigs of each species were further anchored onto 15 pseudochromosomes, covering 98.3, 99.1 and 99.3% of the assembled sequences (Figure 1F; Figure S3; Table S3). This outcome was consistent with the chromosome number identified by karyotype analyses ($2n = 30$) (Li et al., 2017). The overall percentage of reads mapped from the genomic sequences to the assembled genomes exceeded 97% across each assembly (Table S2). Furthermore, RNA-seq reads from multiple tissues were generated and mapped to the assembled genomes, with more than 90% of these reads mapped across each assembly (Table S2). The high completeness of these assemblies was also evidenced by 98.9, 97.1 and 96.9% BUSCO recovery scores, respectively (Table S3). In total, we identified 72.3, 58.4 and 57.5% of the TvD, TsV and TsJ genomes as transposable elements, respectively, and long terminal repeat retrotransposons (LTR-RTs) dominated the TEs (Table S5). A total of 38 155, 41 662 and 44 768 protein-coding genes were predicted for TvD, TsV and TsJ, respectively, and 94.4, 92.2 and 94.3% of the genes were functionally annotated, respectively (Table S6).

Phylogeny, gene families, and genome evolution in Anacardiaceae

Toxicodendron belongs to the Anacardiaceae family (Figure 2A; Figure S4). Genomic analysis of species within Sapindales from Sapindaceae, Anacardiaceae and Rutaceae revealed that 564 gene families were unique to *Toxicodendron* (Figure 2B). The KEGG enrichment results showed that *Toxicodendron*-specific genes were significantly enriched in pathways such as linoleic acid metabolism, glycosaminoglycan degradation, and brassinosteroid biosynthesis (Table S7). Further comparison among four

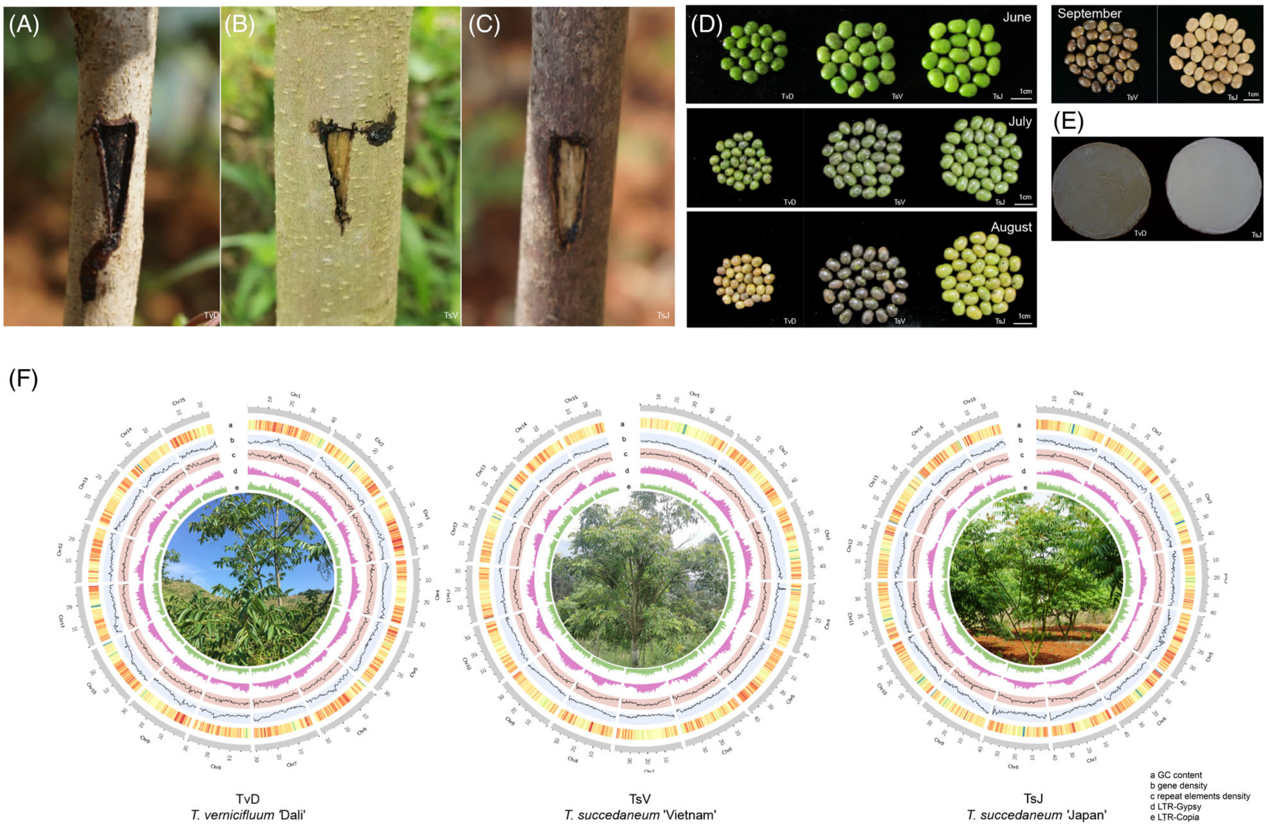

Figure 1. Characteristics of the genomes of three *Toxicodendron* cultivars.
(A–C) Photos of the raw lacquer derived from the phloem tissue of three *Toxicodendron* trees.
(D) Comparison of fruit size among three *Toxicodendron* trees from June to September.
(E) Comparison of *Toxicodendron* wax between lacquer trees (TvD) and wax trees (TsJ).
(F) Genomic characteristics of three *Toxicodendron*s. The tracks from the outer to the inner circle are the chromosomes: a, GC content; b, gene density; c, repeat element density; d, LTR-Gypsy distribution; and e, LTR-Copia distribution.

individuals indicated that a core set of 16 984 gene families were shared by *Toxicodendron*, whereas 390, 358, 282, and 422 gene families were unique to TvC, TvD, TsV and TsJ, respectively (Figure 2B). Compared with the MRCAs of *Toxicodendron* (*T. vernicifluum* and *T. succedaneum*) and *Pistacia* (*P. vera*), a total of 239 expanded and 106 contracted orthogroups were observed in the ancestor of *Toxicodendron* (Figure 2A; Figure S5), and further KEGG enrichment revealed that expanded gene families were predominant in 2-oxocarboxylic acid metabolism, flavonoid biosynthesis, and alpha-linolenic acid metabolism (Table S8), echoing the known features that *Toxicodendron* specializes in the synthesis of secondary metabolites such as urushiol and lipids (Tong et al., 2019).

To investigate the whole-genome duplication (WGD) of Anacardiaceae, the number of synonymous substitutions per synonymous site (Ks) was characterized (Figure 2C; Figures S6 and S7). The Ks distributions of all paralogous gene pairs were almost the same for both *Mangifera indica* and *Anacardium occidentale* (peak at ~0.35), suggesting that a recent WGD event occurred before the split between *Anacardium* and *Mangifera* (Figure 2C). The Ks peak values of paralogous gene pairs from three *Toxicodendron* trees, *Pistacia vera* and *Sclerocarya birrea*, were all approximately 1.5 (Figure 2C; Figure S6), which is similar to those of species from Sapindaceae (*Lichi*, *Acer*, and *Xanthocerase*) and Rutaceae (*Citrus*) (Hu et al., 2022), indicating the absence of further WGDs in most species of Sapindales since the ancient gamma triplication event (Wang et al., 2020). Additionally, syntenic depth ratios of 2:2:1 among *M. indica*, *A. occidentale* and *Toxicodendron* (*T. vernicifluum* and *T. succedaneum*) (Figure S8) also provided additional evidence for a recent WGD event in the common ancestor of *Anacardium* and *Mangifera* but not in *Toxicodendron*. Notably, all the Anacardiaceae genomes displayed a peak Ks value <0.1 (Figure 2C; Figure S6), which might have resulted from recent local duplications (including segmental duplication and tandem duplication), and our results are consistent with those of earlier reports on Sapindaceae genomes (Zheng et al., 2022) (Figure S9). KEGG enrichment analysis indicated that the local duplications of *Toxicodendron*

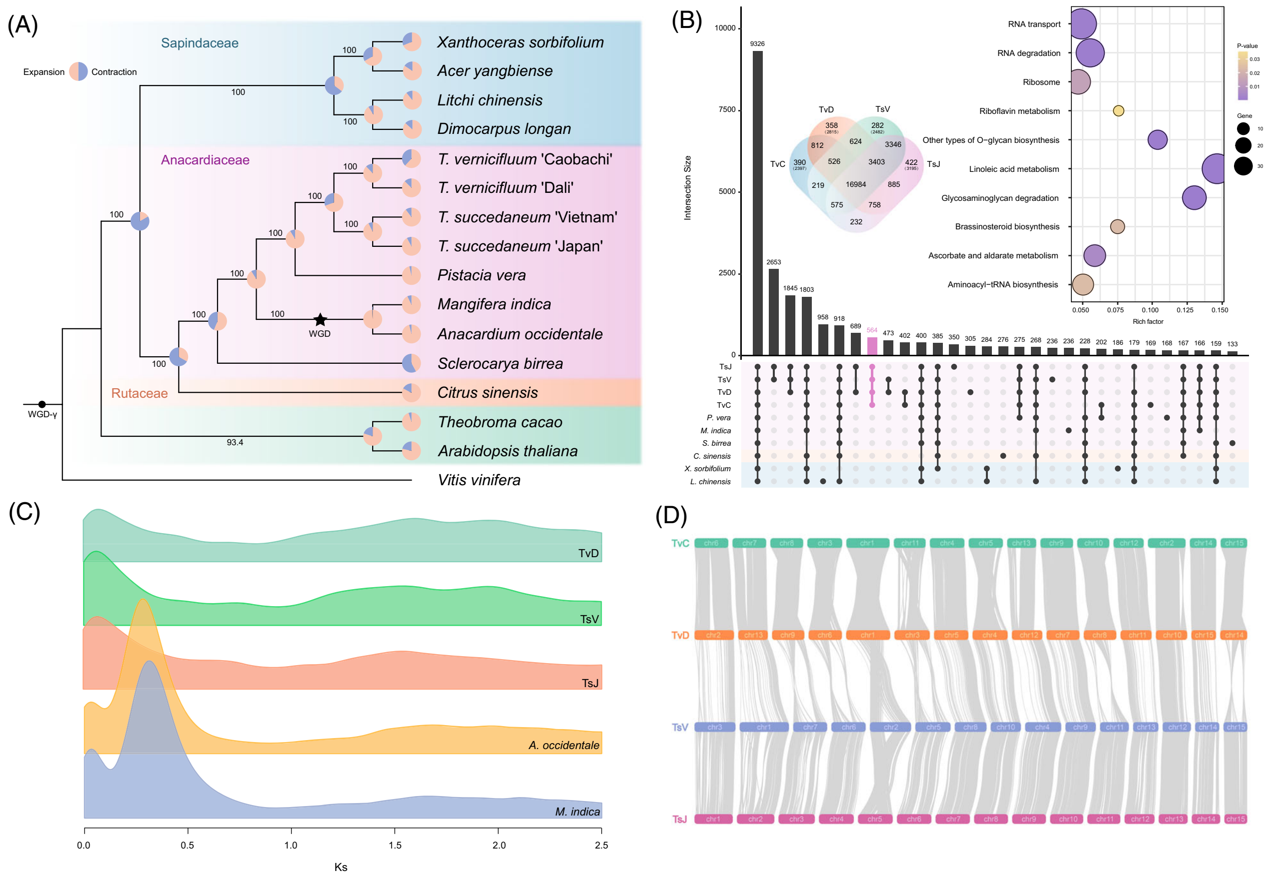

Figure 2. Evolutionary analysis of three *Toxicodendron* genomes.

(A) Phylogenetic analysis of two *Toxicodendron* species among selected plants. The maximum likelihood tree was generated from 414 single-copy orthologous genes. WGT-γ, a whole-genome triplication event in early eudicots; WGD, the most recent WGD event that may have occurred in the common ancestor of *Mangifera* and *Anacardium*. The ratios of expanded and contracted gene family numbers in each evolutionary node are shown in the pie chart, and the numbers are shown in Figure S5.

(B) An UpSet plot showing the number of unique gene families for two *Toxicodendron* species among the selected plants, and their KEGG enrichment is shown in the scatterplot. The Venn diagram shows the commonly shared gene family numbers in the three *Toxicodendron* genomes.

(C) Ks distribution of syntenic orthologs from three *Toxicodendron* cultivars (TvD, TsV, and TsJ), *Anacardium occidentale* and *Mangifera indica*. The y-axis shows the ratio of gene pairs in the syntenic block. The WGD-Ks peak values of *Mangifera* and *Anacardium* were ~0.35, and the peak Ks value was <0.1, which might have resulted from recent local duplications.

(D) Genome collinearity analysis among four *Toxicodendron* genomes.

were associated with ubiquitin-mediated proteolysis, FA elongation, linoleic acid metabolism, and phenylpropanoid biosynthesis (Table S9).

To further investigate genome evolution in *Toxicodendron* species, we examined the collinear relationships and structural variations among TvC, TvD, TsV, and TsJ. TvC and TvD exhibited a sister relationship with TsV and TsJ, which was supported by the high bootstrap value (BS = 100) (Figure 2A; Figure S4). In general, the genomes of the two species were almost perfectly collinear, but more rearrangements or structural variations (SVs) were detected between *T. vernicifluum* (TvC and TvD) than between *T. succedaneum* (TsV and TsJ) (Figure 2D; Figure S10). Additionally, a greater number of presence/absence variations (PAVs) were detected between species, and most of them were located in intergenic and repeating regions (Figure S11; Table S10).

Multiomics studies on the differential urushiol production capacity among *Toxicodendrons*

To compare the urushiol production capacity among the various tissues of the three cultivars, we investigated the production of various types of urushiol (including urushiol I-IV, urushiol [15:3] and laccol) in the phloem and leaves (Figure 3A), by performing a widely targeted metabolomics analysis strategy for polyphenol and flavonoid detection and by using an LC–MS/MS platform to identify them. We found that most types of urushiol in TvD were significantly more abundant than those in TsV and TsJ. The contents of most types of urushiol (apart from urushiol

III) were markedly greater in the phelom than in its leaves (see ANOVA in Table S11). This evidence supports the phenotypic difference in the production capacity of urushiol among TvD, TsV and TsJ (Figure 1A–C) and further confirms that TvD is a highly urushiol-producing species.

Given the importance of the *PKS* family in urushiol production and its role in the coordination of FA metabolism-related enzymes (Bai et al., 2018, 2022; Weisberg, 2014) (Figure 3B), we identified 27, 24 and 29 *PKS/CHS* homologs from the genomes of TvD, TsV and TsJ, respectively, which showed similar gene numbers to those of *P. vera* (23) and *M. indica* (27) (Figure 3C; Figure S12; Table S12). Further phylogenetic analysis revealed that the *PKS/CHS* family could be divided into five groups, *namely*, the *CHS1-4* family and the other *PKS family* (*referred to hereinafter as the CHS-like family*). Intriguingly, the TvD genome cannot encode *CHS1*, but two copies of *CHS1* were identified in the genomes of both TsV and TsJ, suggesting that the *CHS1* clade might not be involved in urushiol biosynthesis in *Toxicodendron*. All three *Toxicodendron* genomes contained a single copy of the *CHS2* ortholog, and low expression levels of *CHS2* were detected in the phloem tissue of the three *Toxicodendron* cultivars, which indicated that *CHS2* might not explain the increased urushiol synthesis in TvD. The *CHS3* and *CHS4* clades were distributed in both Spindaceae and Anacardiaceae but not in Rutaceae, which implied that these two clades might have originated at the common ancestor of Sapindales but were lost in Rutaceae. Additionally, a remarkable expansion of *CHS4* occurred in parts of Anacardiaceae plants, such as *Toxicodendron* and *Anacardium*.

The gene expression results revealed that two of the three *CHSL*s of TvD exhibited greater expression in the phloem than in the leaf (Figure 3D; Table S13), which coincided with the urushiol level in the two tissues. Moreover, these two *CHSL*s, but not the other types of *CHS*s, exhibited coexpression correlations with both *KCS* and *ACSL* in the TvD variety (Figure 3E), and both genes participate in FA metabolism and provide substrates for downstream *CHS* to further produce urushiol. Based on the above analysis, *CHSL* may play a critical role in the accumulation of urushiol in phloem tissue.

Influence of metabolic flux switching on urushiol accumulation

The regulation of metabolic flux may also affect metabolite accumulation. The intermediates of FFA metabolism are involved in the formation of urushiol (Figure 3B). We detected that the FFA levels in the phloem were greater in TvD than in TsV and TsJ (Figure 3F; Table S14; ANOVA, P value <0.01), suggesting that more substrates were supplied for subsequent urushiol biosynthesis, which resulted in greater urushiol accumulation in TvD than in TsV and TsJ. Therefore, we assumed that a high FA content in the phloem also promotes the urushiol production capacity of TvD.

With respect to *CHS*s, they not only utilize various long FA-CoA substrates but also use coumaroyl-CoA as a substrate to produce chalcone (Austin & Noel, 2003). We compared the various types of chalcone in the phloem among TvD, TsV and TsJ, and detected greater concentrations of various types of chalcones in the phloem of TsJ than in TvD's phloem (Figure 3G; Table S15; ANOVA, P value <0.01). Moreover, the concentration of total chalcone in the leaves of TvD was greater than that in the phloem of TvD (Table S15; ANOVA, P value <0.01). In addition, the phenotypes of TvD showed that the urushiol level was higher in the phloem than in the leaf, while the chalcone level in the phloem was lower than in the leaf (Figure 3A, G). This suggests that the urushiol metabolic pathway is more active in the phloem, whereas the chalcone metabolic pathway is more active in the leaves of TvD. Our findings also indicate that because the FFA and chalcone metabolic pathways partially overlap and intersect with the urushiol metabolic pathway to some extent, variations in FFA and chalcone metabolism could contribute to the differences in urushiol accumulation observed between the two *Toxicodendron* species (Figure 3H).

Lipidomic analysis of fruit development

Based on the comparative lipidome, we detected differences in the duration of lipid accumulation among the three cultivars. We found that (1) During the developmental stage, the total lipid content of fruits from TvD and TsJ exhibited a significant increase from June to July (Figure 4B), resulting from an increase in glycerolipid (GL) content (Figure S13). In contrast, the fruits of TsV did not display a similar trend and showed no change in total lipid content from June to July (Figure 4B). (2) In July, the total lipid content of fruits of TsV was significantly lower than that of TvD and TsJ (Figure S14), which might be caused by the increased water content of its fruits than that of TvD and TsJ (Figure S21; Table S26). (3) The total lipid content of TsJ's fruits in June was significantly higher than that of TvD and TsV, indicating a higher total lipid content at the initial developmental stage (Figure S14). (4) When the fruits of the three cultivars from the late developmental stage were compared with those from the ripe stage (from August to September for TsV and TsJ, and from July to August for TvD), the total lipid content of TvD increased significantly, whereas that of TsV did not significantly change, and that of TsJ significantly decreased (Figure 4B). Similarly, a comparison of the lipid metabolism-related genes revealed gene expansion in TsJ compared with TvD in the fatty acid biosynthesis, wax biosynthesis and Kennedy pathways (Figure 4E; Table S17). For example, *fatty acyl-CoA reductase* (*FAR*), *long-chain-alcohol oxidase*

(*FAO*) and *long-chain-alcohol O-fatty-acyltransferase* (*WASX*) catalyze the last two steps of wax-ester metabolism (Cheng et al., 2004; Doan et al., 2009; Patwari et al., 2019) (Figure 4F; Figures S15–S17).

We then compared the differences in lipid composition between developing and ripe fruits among the three cultivars (Figure 4B; Table S16). Total lipids are classified into five main types: free fatty acids (FFAs),

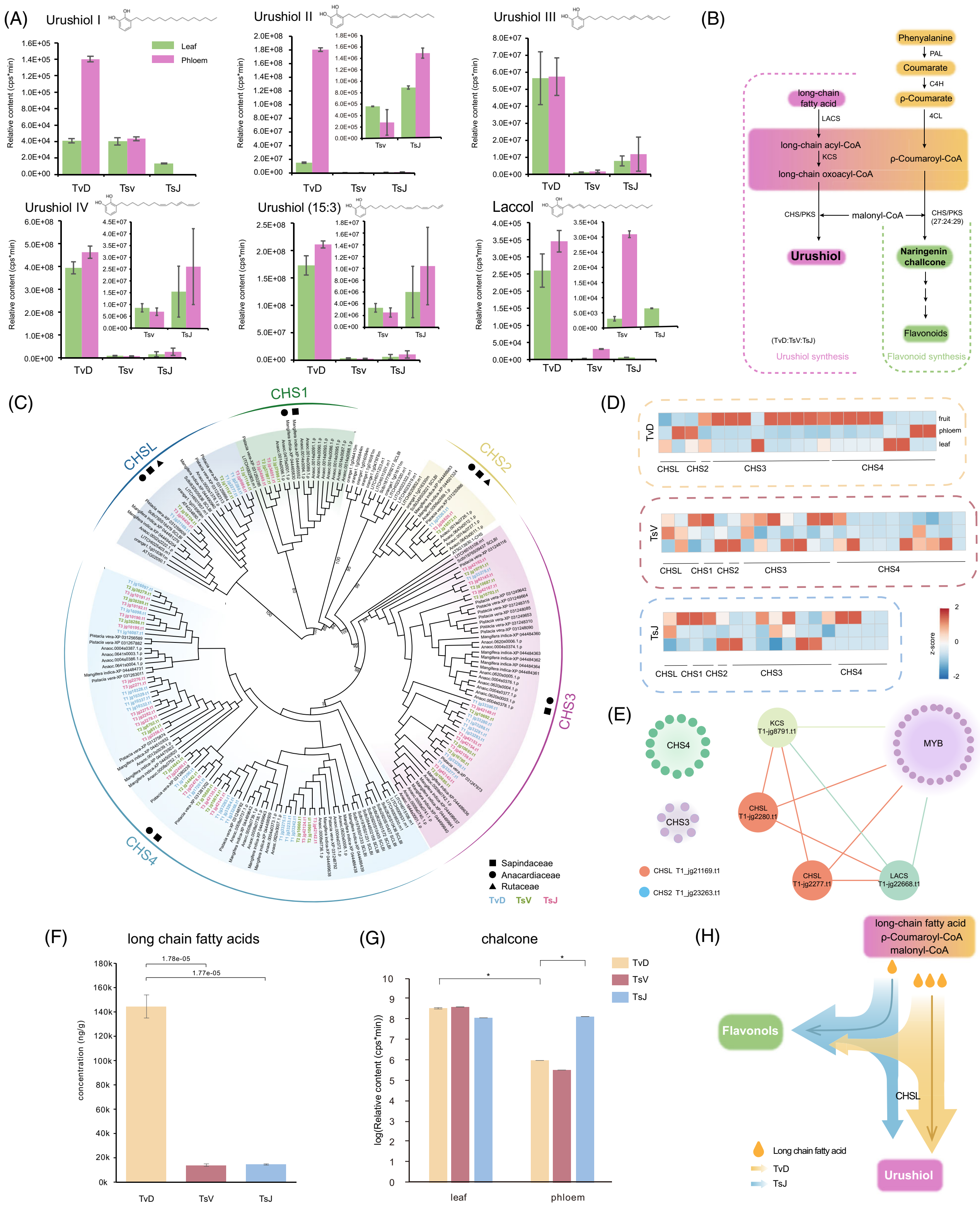

Figure 3. Multiomics study on differential urushiol accumulation among *Toxicodendron*s.
(A) Comparison of the contents of various kinds of urushiol among different tissues of three *Toxicodendron* cultivars.
(B) Putative biosynthetic pathway of urushiols in *Toxicodendron*. The abbreviations of the gene names can be found in Table S29. The gene copy numbers of TvD, TsV, and TsJ are shown in brackets.
(C) Maximum likelihood phylogenetic tree of the PKS/CHS family of selected species using amino acids.
(D) The normalized gene expression level of the CHS gene family among different tissues of three *Toxicodendron* cultivars.
(E) Predicted regulatory network and connections among CHS1-4, CHSL, MYBs and selected genes involved in urushiol biosynthesis pathways.
(F) Comparison of long-chain fatty acids of phloem among TvD, TsV, and TsJ.
(G) Comparison of the chalcone concentration of leaf and phloem among TvD, TsV, and TsJ. *, adjusted *P* value <0.05.
(H) Putative model to explain the difference in urushiol accumulation among *Toxicodendron species*.
The error bars indicate the means ± SDs.

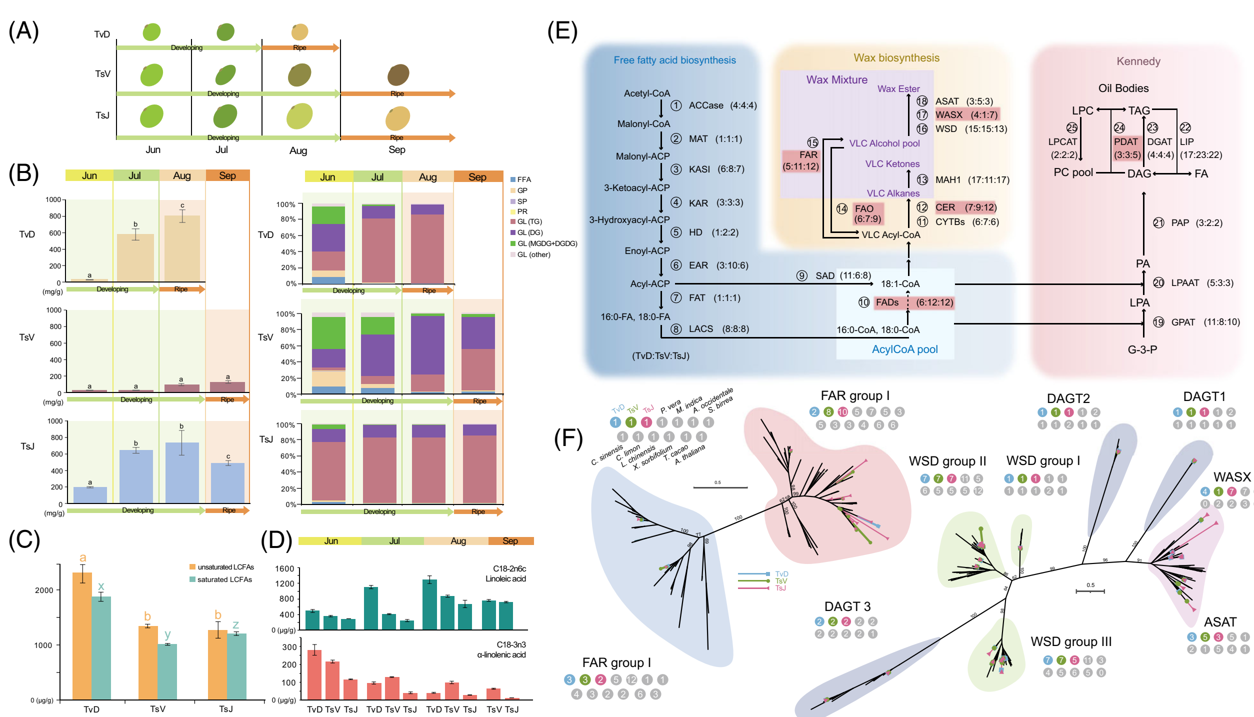

Figure 4. Molecular mechanisms involved in the high production of *Toxicodendron* wax and seed oil in Wax trees.
(A) Diagram of fruit development and ripening. The development period of TvD is June and July, and the ripening period is August. The development period of TsV and TsV is from June to August, and the ripening period is September.
(B) Comparison of total and individual lipid concentrations (left) and percentages (right) of fruits among three *Toxicodendron* cultivars.
(C) Comparison of unsaturated and saturated LCFA concentrations in fruits among three *Toxicodendron* cultivars.
(D) Comparison of the concentration of each free fatty acid among the three *Toxicodendron* cultivars.
(E) Schematics of the free fatty acid biosynthesis, wax biosynthesis and Kennedy pathways in *Toxicodendron*. The gene copy number of each catalytic step of TvD, TsV, and TsJ is shown within brackets. The abbreviations of the gene names can be found in Table S29. The red rectangles indicate that the number of this gene in TsJ was 1.5 times greater than the number in TvD.
(F) Maximum likelihood phylogenetic trees of the FAR gene family (left panel) and wax-ester biosynthesis-related genes (right panel) of the selected species using amino acids. The numbers in the colored or gray circle represent the gene copy number of each clade in each species.
The error bars indicate ± SDs. Jun, June; Jul, July; Aug, August; Sep, September.

glycerophospholipids (GPs), sphingolipids (Guijas et al., 2018), glycerolipids (GLs) and penolol lipids (PRs) (Chen et al., 2022). The lipid composition of TsJ did not change significantly from the developing fruits to the ripe fruits. In the developing fruits of TsV, galactolipids (MGDG + DGDG) and diglycerides (DGs) were the predominant lipid types in June and July, but triglyceride (TG) levels increased dramatically and constituted ~80% of the total oil in the ripe fruits. The lipid composition of TvD changed greatly from June to July (see ANOVA in Table S16); for example, the percentage of TG concentration increased from 36.5 to 86.6%.

The proportion of FFAs was greater only in the developing fruits of the three cultivars in June (>1% in TsJ; >6% in TvD and TsV) but dramatically decreased in the ripe fruits (Figure 4B; Tables S16 and S18). In terms of the FFA concentration rather than the proportion, TvD continuously accumulated as the fruits developed, but dynamic changes in the FFA concentration were observed for both TsV and TsJ (Figure S13). Moreover, our results showed that long-chain fatty acids (LCFAs, C13-C21) are the main components of FFAs in fruits. The concentrations of both polyunsaturated and saturated LCFAs in the ripe fruits of TvD were greater than those in the ripe fruits of TsV and TsJ (Figure 4C; Table S18). Linoleic acid (C18:2) and α-linolenic acid (C18:3) are valuable polyunsaturated long-chain fatty acids (LCFAs) that contribute to human health (Bemelmans et al., 2000). Our investigation revealed consistently elevated levels of these two types of polyunsaturated fatty acids (PUFAs) in TvD compared with those in TsV and TsJ across various stages of fruit development (Figure 4D; Table S18). This suggests that despite its small size (Table S19), TvD serves as a substantial and nutritious source of these essential PUFAs.

The regulation of lipid accumulation in *Toxicodendron*

Based on WGCNA, 4, 11, and 23 coexpression modules were identified in the three cultivars, respectively (Figure 5; Table S20). Differential gene expression was observed between June and September among the three cultivars. The majority of genes in the developing fruit of TsJ were highly expressed in both June and July (Figure 5A), whereas more genes in the developing fruit of TsV were highly expressed only in June (Figure 5B). In June, the development of TvD was relatively short, and many genes exhibited high transcription levels (Figure 5C).

To understand the differences in the expression patterns, KEGG enrichment of each module for the three cultivars was performed (Figure 5). We found that 'sphingolipid metabolism' was enriched in M1 of TsJ, but both 'FA metabolism' and 'FA biosynthesis' were enriched in M4, where all genes were highly expressed only in June and July. Additionally, 'glycerolipid metabolism', 'FA degradation' and 'ether lipid metabolism' were found to be enriched in M17 of TsJ, and most genes in this module were highly expressed in August. In contrast to TsJ, genes related to 'FA metabolism' and 'FA biosynthesis' were predominant in TsV fruits in both July and August (M3 and M5). Only four coexpression modules were identified from the TvD WGCNA, and although no lipid-associated metabolism was found from KEGG enrichment, gene ontology enrichment showed that the 'FA biosynthetic process' and 'FA metabolic process' were metabolically active only in June (Figure S18).

Our WGCNA also revealed that the FFA biosynthetic pathway, rather than wax biosynthesis and Kennedy metabolism, was predominant in terms of fruit lipid accumulation (Figure S19). The lipid accumulation of TsJ occurred mainly in June and July; consistently, genes from the FFA biosynthetic pathway were also highly expressed overall during the 2 months (Figures 4A and 5B; Table S21). Similarly, higher transcription levels of genes (such as ACCase, MAT, and HD) in the FFA biosynthetic pathway strongly coincided with the rapid accumulation of total lipids in TsV fruits in August.

To further understand how lipid metabolism is regulated, we investigated the interactions between transcription factors (TFs) and genes involved in lipid metabolism. Our results suggested that TF-mediated regulation of lipid metabolism differed among the three cultivars, which was supported by the difference in the number of genes expressed each month among the three cultivars (Figure 6; Figure S20). A total of 17, 13 and 15 time-series expression levels centering on TFs were finally reconstructed, and a coexpression network involving the 886, 844 and 804 differentially expressed TFs and 96, 100 and 94 genes from the lipid metabolism of TvD, TsV and TsJ, respectively, was constructed (Table S22). Lipid metabolism in TvD and TsV fruits was regulated primarily in June and August, whereas such regulation in TsJ was highly active in June, July, and September. These findings suggested that these 3 months were potential key time points for the rapid changes in lipids in TsJ fruits.

With respect to TsJ, we found that many highly expressed genes from FFA biosynthetic pathways were regulated by *MYB* family genes in June, for example, six out of seven copies of *KASI* had coexpression correlations with 15 *MYB*s (Figure 6A,B; Table S22). Compared with those in September, more genes in the wax biosynthesis pathway were regulated in June and July (Figure 6C). The main TFs involved in this regulation are bHLH, MYB, and NAC (Table S22), but they may be regulated in different ways. For example, *CER* is a crucial gene for wax metabolism, and we found that *MYB*s were mainly responsible for the regulation of *CER* in June, whereas no *MYB*s were involved in CER regulation in July (mainly *NF-YB*s) (Table S23). Lipase, a key enzyme involved in lipid degradation and transformation, was found to be more strongly regulated by TFs in September (Figure 6D). Similarly, the total lipid concentration of the ripe fruits of TsJ decreased significantly in September. Further examination revealed that these highly expressed lipases in September were regulated mainly by AP/ERFs. The three lipases with the highest expression levels (T3_jg10400.t1, T3_jg38768.t1 and T3_jg40103.t1) interacted with 17, 12 and 10 AP/ERFs,

Figure 5. Gene coexpression modules over the course of fruit development and expression profiles of genes related to lipid metabolism.
(A–C) The left panel is a heatmap showing the relative expression of genes in 4, 11, and 23 coexpression modules across different times among *Toxicodendron* cultivars (from top to bottom: TsJ, TsV, and TvD). The heatmaps indicate the normalized expression values (z scores) of genes related to the fatty acid biosynthetic pathway across different times among the three *Toxicodendron* cultivars. From top to bottom are TsJ, TsV, and TvD.


(A)
M1
M2
M3
M4
M5
M6
M7
M8
M9
M10
M11
M12
M13
M14
M15
M16
M17
M18
M19
M20
M21
M22
M23
TsJ Jun
TsJ Jul
TsJ Aug
TsJ Sep
Sphingolipid metabolism
Other glycan degradation
Porphyrin and chlorophyll metabolism
Glycolysis / Gluconeogenesis
Carbon metabolism
N−Glycan biosynthesis
Various types of N−glycan biosynthesis
Fatty acid metabolism
Fatty acid biosynthesis
Lipoic acid metabolism
Biotin metabolism
Photosynthesis − antenna proteins
Biosynthesis of amino acids
Glycine, serine and threonine metabolism
Monobactam biosynthesis
Propanoate metabolism
Proteasome
One carbon pool by folate
Inositol phosphate metabolism
Lysine biosynthesis
Peroxisome
Fructose and mannose metabolism
GPI−anchor biosynthesis
Ribosome
Plant hormone signal transduction
Limonene and pinene degradation
Valine, leucine and isoleucine degradation
Glycerolipid metabolism
Histidine metabolism
Lysine degradation
beta−Alanine metabolism
Fatty acid degradation
Ether lipid metabolism
Taurine and hypotaurine metabolism
Ribosome biogenesis in eukaryotes
Spliceosome
RNA transport
Ribosome
Protein processing in endoplasmic reticulum
Spliceosome
−log10(Q value)
2.5
5.0
7.5
10.0
0.00
0.25
0.50
0.75
1.00
Free fatty acid biosynthesis
ACCase
MAT
KASI
KAR
HD
EAR
FAT
LACS
SAD
FAD6
Jun
Jul
Aug
Sep
2
0
-2
(B)
M1
M2
M3
M4
M5
M6
M7
M8
M9
M10
M11
TsV Jun
TsV Jul
TsV Aug
TsV Sep
Ribosome
Porphyrin and chlorophyll metabolism
GPI−anchor biosynthesis
Photosynthesis − antenna proteins
N−Glycan biosynthesis
One carbon pool by folate
Other glycan degradation
Base excision repair
Basal transcription factors
Glycine, serine and threonine metabolism
Purine metabolism
Glycolysis / Gluconeogenesis
Biosynthesis of amino acids
Carbon metabolism
Fatty acid metabolism
Fatty acid biosynthesis
Glycolysis / Gluconeogenesis
Biotin metabolism
Peroxisome
Synthesis and degradation of ketone bodies
Limonene and pinene degradation
Endocytosis
Pyruvate metabolism
Fatty acid biosynthesis
Selenocompound metabolism
Biosynthesis of secondary metabolites
Metabolic pathways
Flavonoid biosynthesis
Glutathione metabolism
−log10(Q value)
5
10
15
20
25
0.2
0.4
0.6
0.8
ACCase
MAT
KASI
KAR
HD
EAR
FAT
LACS
SAD
FAD6
Jun
Jul
Aug
Sep
2
0
-2
(C)
M1
M2
M3
M4
TvD Jun
TvD Jul
TvD Aug
Porphyrin and chlorophyll metabolism
Phagosome
Glycine, serine and threonine metabolism
Phosphatidylinositol signaling system
Glycerophospholipid metabolism
Inositol phosphate metabolism
Photosynthesis − antenna proteins
beta−Alanine metabolism
Biosynthesis of amino acids
Cysteine and methionine metabolism
Vitamin B6 metabolism
Selenocompound metabolism
Phenylalanine, tyrosine, tryptophan biosynthesis
Proteasome
Limonene and pinene degradation
Ubiquitin mediated proteolysis
Ribosome
Spliceosome
Ribosome biogenesis in eukaryotes
mRNA surveillance pathway
Basal transcription factors
−log10(Q value)
5
10
15
0.25
0.50
0.75
ratio
ACCase
MAT
KASI
KAR
HD
EAR
FAT
LACS
SAD
FAD6
Jun
Jul
Aug
2
0
-2

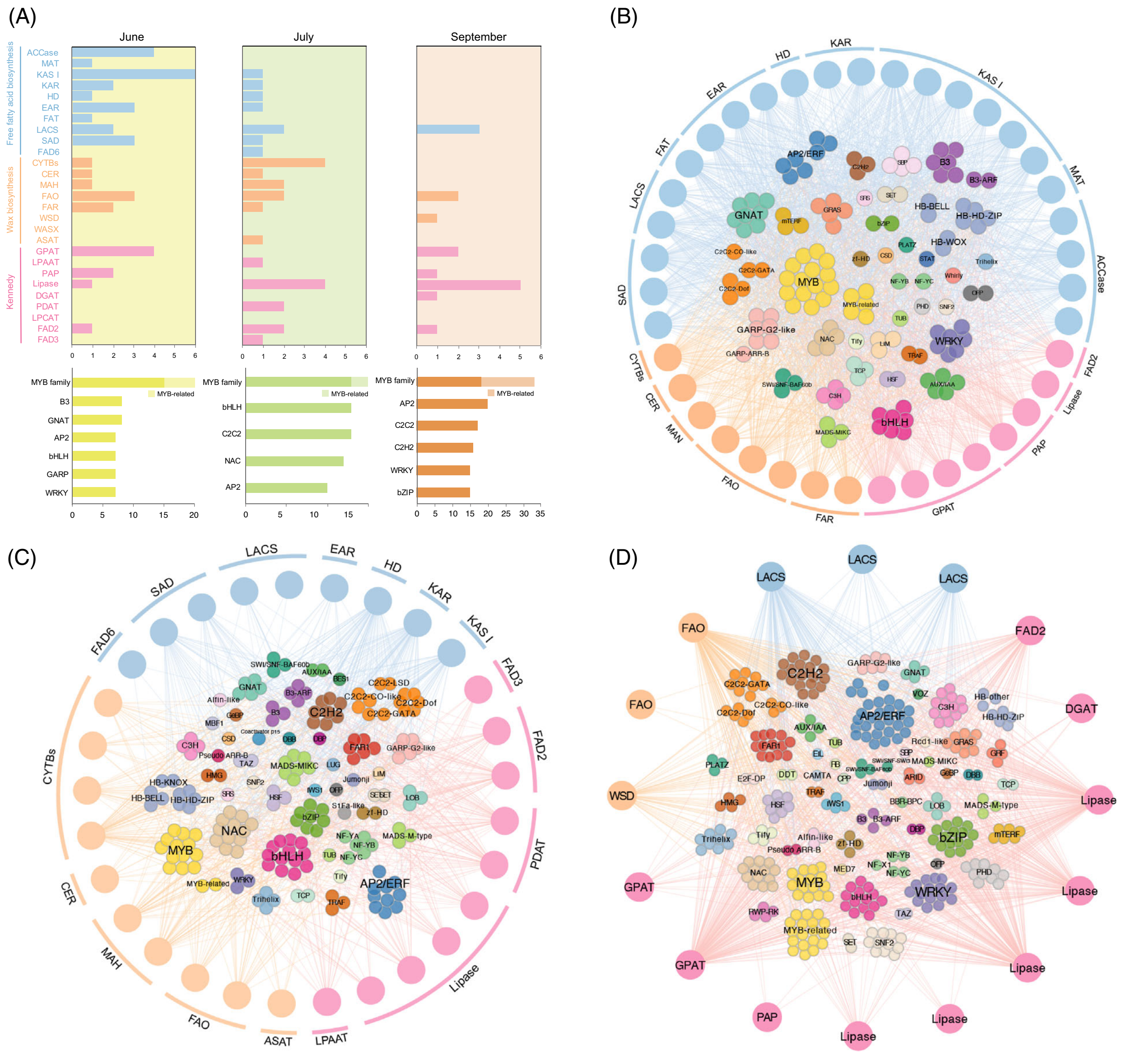

Figure 6. Time-ordered gene coexpression network related to lipid accumulation over the course of TsJ fruit development.
(A) Comparison of the numbers of TFs and genes of TsJ involved in biosynthetic pathways for FFA, wax and Kennedy from TO-GCNs in June, July and September, respectively. The largest number of TFS are displayed.
(B) Subnetwork of TsJ for lipid metabolism in June.
(C) Subnetwork of TsJ for lipid metabolism in July.
(D) Subnetwork of TsJ for lipid metabolism in September. Outer ring: blue, orange and pink circles denote genes involved in the biosynthetic pathways of FFAs, wax and Kennedy, respectively. The inner circles denote the various types of TFs.

respectively, which was far greater than the number of interactions with other TFs.

DISCUSSION

Genome evolution in *Toxicodendron*

Here, we constructed high-quality reference genome assemblies for three commercially important *Toxicodendron* species, *T. vernicifluum* 'Dali', *T. succedaneum* 'Vietnam' and *T. succedaneum* 'Japan'. Comparative genomics analyses revealed high collinearity between *T. vernicifluum* 'Dali' and the previously published *T. vernicifluum* 'Caobachi''s genome (Bai et al., 2022) (Figure 2D). Our assembled genome size was close to its estimated size based on k-mer analysis, and the contig N50 length was 18.8 Mb, nearly three times greater than that of the *T. vernicifluum* 'Caobachi' genome (Table S24). Notably, the BUSCO of our gene set increased by 4% compared with that of *T. vernicifluum* 'Caobachi' (from 93.6 to 97.6%; Table S24). The LTR assembly index (LAI) of our genome (15.68) was greater than that of the published genome (14.05).

The results of collinear relationships and structural variation analyses revealed large genomic differences between *T. vernicifluum* and *T. succedaneum*, and combined with phylogenetic relationships, these findings suggested that they may be two different species, while fewer genomic structural variations between the two *T. vernicifluum* strains and between the two *T.* succedaneum strains were identified; therefore, they are more likely to be different cultivars.

We next compared the gene families between TvD and *T. vernicifluum* 'Caobachi'. We found that a total of 18 167 gene families were shared, and TvD exhibited 3831 unique gene families involved in pathways such as '2-oxocarboxylic acid metabolism', 'linoleic acid metabolism', and 'diterpenoid biosynthesis', and *T. vernicifluum* 'Caobachi' had 2778 unique gene families related to pathways such as 'phagosome' and 'biosynthesis of unsaturated FAs' (Table S25), implying that there was a difference in metabolism between the two cultivars.

We found that all the *Toxicodendron* and other Anacardiaceae genomes displayed a peak at Ks <0.1 (Figure 2C), which probably resulted from recent local duplications, which is consistent with earlier reports (Zheng et al., 2022) (Figures S6 and S9). These locally duplicated genes in *Toxicodendron* are associated with pathways such as FA metabolism, flavonoid biosynthesis and phytohormone signal transduction, which might be involved in urushiol and lipid metabolism. A similar absence of WGDs after the early eudicot whole-genome triplication event in many Sapindales followed by local duplication has been shown to promote genetic diversity; for example, local duplication caused the expansion of resistance genes in the *Nephelium lappaceum* genome and enhanced its stress resistance (Zheng et al., 2022).

Differential urushiol production capacity between *T. vernicifluum* and *T. succedaneum*

The contents of various kinds of urushiol are vital traits to consider in the *Toxicodendron* breeding process (Wang et al., 2020) because they are crucial factors in determining both the production and quality of raw lacquer. Our findings confirmed that TvD is a more urushiol-rich species than TsV and TsJ. Compared with non-Anacardiaceae species, most Anacardiaceae species exhibit extensive expansion of *PKS/CHS* genes. However, gene duplication might have occurred after the split with *Sclerocarya* since it encodes fewer *PKS/CHS genes*, and our results agreed with those of previous studies suggesting that *CHS*s might have expanded early in Anacardiaceae (Wang et al., 2020).

Integrated multiomics analyses revealed that CHSL might be the key enzyme involved in urushiol accumulation since the *CHSL*s of TvD exhibited greater expression in the phloem tissue than in the leaves, which is consistent with urushiol levels in the various tissues of TvD. In addition, the coexpression network of genes upstream of urushiol-related metabolism in the TvD phloem revealed that *CHSL*s were the only PKS clade that associated with FFA metabolism-related genes and a large number of MYBs (Figure 3E). MYBs were previously reported to be key transcription factors involved in the regulation of flavonoid, FA, and polyphenol metabolism (Czemmel et al., 2012; Lin et al., 2017; Miyamoto et al., 2020). Therefore, we inferred that the MYB family is potentially a key upstream regulator of urushiol-related metabolism in the TvD phloem. In addition, as a key upstream substrate for urushiol biosynthesis (Bai et al., 2022), a greater level of LCFAs in the phloem of TvD than in that of TsV and TsJ might supply enough substrate to promote subsequent urushiol biosynthesis in TvD (Figure 3F). Interestingly, more chalcones were detected in the phloem of TsV and TsJ than in that of TvD (Figure 3G), suggesting that the PKS/CHSs of TsV and TsJ are involved mainly in chalcone metabolism. Notably, other types of CHSs cannot be excluded from the possibility of participating in the biosynthesis of urushiol; for example, clade III CHSs were found to be related to urushiol biosynthesis in the peel of mango (Wang et al., 2020).

Specific lipid accumulation and regulation in *T. succedaneum* 'Japan'

Our results confirmed that the total lipid concentration of TsJ was greater and that the lipid composition of the fruit differed among the three individuals (Figure 4). A higher concentration of unsaturated LCFAs in TvD fruits might cause lower antioxidation activity than in TsJ fruits, which might explain the darker color phenotype of the wax of TvD fruits than that of the wax of TsJ fruits because more unsaturated LCFAs are more susceptible to oxidation (Figure 1E). The duplication of genes associated with the elongation of very-long-chain fatty acids in TsJ (4 copies) compared with TvD (2 copies) may be associated with higher contents of very-LCFAs in TsJ than in TvD and TsV (Tables S17 and S18).

Wax is extracted from the fruit peel of the wax tree TsJ, and we investigated the genes associated with the biosynthesis of cuticle waxes that are primarily composed of very-long-chain alkanes (Ai et al., 2022). *ECERIFERUM1* (*CER1*) is recognized as the core element for very-long-chain alkane biosynthesis in *Arabidopsis* (Bourdenx et al., 2011). The TsJ genome encoded 7 copies of *CRE1* homologs, which was almost double that of TvD (4) and TsV (3) (Figure 4E; Table S17). Additionally, more duplications of other wax metabolism-related genes (*FAR, FAO2*, and *WASX*) in the TsJ genome might further provide the molecular basis for greater wax accumulation in fruit peels.

A comparison of lipid profiles might reveal that the optimal time to harvest wax tree fruit for industrial application in August rather than in September is due to the dramatic decrease in lipid concentration and weight in September, accompanied by increased protein content (Figure S21; Tables S18, S26, and S27). The negative association between protein and oil production has also been well-documented in soybean seeds (Kambhampati et al., 2021). Although the fruits of TvD were relatively smaller than those of TsV and TsJ, they presented higher concentrations of total lipids, linoleic acid and protein at maturity in August (Figure S21). Therefore, we propose that further improvements in the size of the TvD fruit can greatly promote the development of the *Toxicodendron* industry.

With respect to gene transcription levels, most genes related to lipid metabolism exhibited greater expression in *Toxicodendron* fruits than in other tissues, especially genes related to the FFA biosynthetic pathway (Figure S22; Table S28). We hypothesized that increased FFAs probably further promote the downstream biosynthesis of wax and triacylglyceride (TAG), ultimately contributing to the increased accumulation of lipids in fruits.

Abundant coexpression correlations were detected in June, July, and September in TsJ' fruits. We assumed that the *MYB* family might act as the core regulator to activate the expression of genes (such as *KASI*, a crucial gene regulating growth and FFA synthesis in plants [Wu & Xue, 2010]) from the FFA biosynthetic pathway in June. The regulation of *MYB*s involved in seed oil biosynthesis has also been documented in *Brassica*, soybean and *Camellia* (Li, Huang, et al., 2022; Liu et al., 2014; Rajavel et al., 2021). bHLH, MYB and NAC are the main TFs that regulate wax metabolism in the developing fruit of TsJ in July. These TF families have also been reported to be crucial regulators of wax synthesis (Li et al., 2016; Seo et al., 2011; Verdaguer et al., 2016). Decreases in lipid concentrations in TsJ fruits were caused by highly coexpressed lipases and many *AP/ERF*s in September. Similarly, *AP/ERF*s were reported to be important regulators of lipid metabolism (Gu et al., 2017; Xu et al., 2013). The two most highly expressed lipases are homologous to *Arabidopsis* triacylglycerol lipase and triacylglycerol lipase SDP1. The former might be involved in TAG storage breakdown (El-Kouhen et al., 2005), and the latter might drive the release of FAs from the oil body (Eastmond, 2006). Thus, we propose that AP/ERFs might serve as the primary regulators of lipase in September, maintaining a trade-off between oil and protein in mature seeds and ensuring the survival of seedlings (Ferreira et al., 2009). The identified TFs associated with the regulation of lipid metabolism during fruit development provide a crucial basis for genome-assisted breeding and improvement of lipid accumulation in wax trees. Our results revealed that the dynamic changes in the lipidome strongly coincided with the expression of several lipid pathway-related genes and transcription factors, indicating that timely feedback may occur between the transcriptome and lipidome. However, investigating the lag effects between metabolite accumulation and gene regulation requires carefully designed sampling methods.

In summary, the multiomics-based genome-wide analysis of three *Toxicodendron* trees in this study provides new insights into the different metabolic pathways involved in the production of urushiol and seed oil among the lacquer tree, *T. succedaneum* 'Vietnam' and wax tree. Gene mining from high-quality genomes of *Toxicodendron trees* offers valuable information for facilitating efficient germplasm exploration and improving the economically important traits of the raw lacquer and lipids of *Toxicodendron* trees to meet the increasing demand for natural metabolites.

MATERIALS AND METHODS

Plant material

Samples of three Toxicodendron species were collected from two locations in Yunnan Province, China. All the plant samples were collected during the growing season and immediately processed for further analysis. The 11-year-old *T. vernicifluum* 'Dali' (TvD) and *T. succedaneum* 'Vietnam' (TsV) trees were sampled from a nursery of *Toxicodendron* germplasm resources in Wenshan, Yunnan Province, China (103°25′27″ E, 23°50′52″ N). This region has a low-latitude, north subtropical plateau monsoon climate. The collection site had a longitude of 104°34′20″ E, a latitude of 23°30′8″, and an altitude of approximately 1400 m. The annual average temperature in Yanshan County is 19°C, with an annual rainfall of 900 mm, which is concentrated between May and October. The area experiences a frost-free period of 250–320 days, with mild winters and moderate summers.

Similarly, 11-year-old *T. succedaneum* 'Japan' (TsJ) trees were obtained from the Arboretum of Southwest Forestry University in Kunming, Yunnan Province (102°45′40″ E, 25°3′41″ N), China, which has a low-latitude plateau monsoon climate. The collection site had a longitude of 102.758667, a latitude of 25.059224, and an altitude range of 1891–2100 m. The average annual temperature in Kunming is 14.9°C, with an extreme maximum of 31.5°C and an extreme minimum of −7.8°C. The region receives an average annual precipitation of approximately 1000.5 mm, with the majority falling between May and September. The area experiences 2327.5 h of sunshine per year.

Trees with a diameter of 12–15 cm at breast height were selected from the TvD, TsV, and TsJ populations and used for the study. During the growing season, young leaves from TvD, TsV, and TsJ were collected for DNA sequencing. The trees' leaves, phloem tissues, and developing fruits were collected for transcriptome analyses and polyphenol, flavonoid and lipid detection (Figure S1). Phloem tissue was collected at the bark side after the bark peeled off the stem at a height of 85 cm above the ground. For the time-ordered comparative multiomics study, developing fruits were collected from selected trees at various developmental stages (June, July, August, and September). All three biological replicate samples were collected and immediately stored in liquid nitrogen for analysis.

DNA and RNA sequencing

The genomic DNA was extracted using a modified cetyltrimethylammonium bromide method (Sahu et al., 2012). A NanoDrop™ One UV–Vis spectrophotometer (Thermo Fisher Scientific, Waltham, MA, USA) and a Qubit® 3.0 fluorometer (Invitrogen Ltd., Paisley, UK) were used to quantify the DNA. The 100-bp paired-end (PE) libraries were prepared for short reads on a MGISEQ-2000 platform following the manufacturer's procedures. Oxford Nanopore libraries were prepared by QIAGEN® Genomic and sequenced using a Nanopore PromethION sequencer (using three flow cells). Hi-C libraries were created from the DNA of fresh leaves using MboI restriction enzymes following a previously published method (Xie et al., 2015). Paired-end reads were generated by using MGISEQ-2000.

Total RNA was extracted with a Spectrum Total RNA Kit (Sigma–Aldrich). The transcriptome libraries were prepared using the NEBNext® Ultra™ RNA Library Prep Kit for Illumina and then sequenced on the Illumina HiSeq 2500 platform with 150-bp paired-end (PE) libraries. Trimmomatic-0.38 was used to trim the raw reads, and the parameters used were as follows: ILLUMINACLIP:adapter.fa:2:30:10 LEADING:5 TRAILING:5 HEADCROP:5 CROP:80 SLIDINGWINDOW:5:15 MINLEN:50.

Genome assembly and quality control

A total of 355.73 Gb of clean short reads were obtained from the raw sequencing reads after filtration of the adapters and low-quality reads. Trimming and filtration of low-quality and duplicate reads were performed by using Trimmomatic-0.39. The 17-mer frequencies and distributions were calculated from JELLYFISH software (v2.2.6) (https://github.com/gmarcais/Jellyfish), and GenomeScope (v2.0) was used to estimate the genome size, the abundance of repetitive elements and the rate of heterozygosity (Vurture et al., 2017).

Approximately 131.64 Gb of Nanopore data were used for genome assembly via NextDenovo v2.3.0 (https://github.com/Nextomics/NextDenovo) with default parameters, but the parameters "seed_cutoff" for three individuals (TvD, TsV, and TsJ) were 44k, 37k, and 44k, respectively. The draft assembly was polished by Pilon (Walker et al., 2014) for 3 rounds with short paired-end reads using default parameters. To reduce heterozygous duplication and generate redundant genome sequences, the Purge_Dups pipeline (v. 1.2.3) was used to purge haplotigs and overlaps in assemblies based on read depth. Genome completeness was assessed with the Embryophyta_odb10 database of BUSCO 5.2.2 (Simão et al., 2015). Additionally, DNA reads and transcripts were also mapped to the draft assembly by using BLAT v.36 (Kent, 2002) and STAR 2.7.6a (Dobin et al., 2013), respectively. Finally, the genome assembly was oriented toward pseudochromosomes based on HiC data (see Methods S1).

Genome annotation

For repeat element annotation, tandem repeats were predicted using Tandem Repeat Finder (4.07). Transposable elements throughout the genome were identified by a combination of homology-based and de novo approaches. For the de novo-based approach, ltr_finder v1.06 (Xu & Wang, 2007), LTR_retriever (Ou & Jiang, 2018), PILER v1.0 (Edgar & Myers, 2005), and RepeatModeler open-1.0.8 were applied to construct repeat libraries, which were combined with RepeatMasker open-4.0.6 (http://www.repeatmasker.org). The software RepeatMasker open-4.0.6 and RepeatProteinMask were applied to identify repetitive sequences using Repbase 22.01 as the homolog-based approach. The LAI value was calculated by LTR_retriever.

Gene structure annotation was carried out after masking the repeat element regions of the genome. BRAKER 2.1.5 (Hoff et al., 2016) was used to predict genes. We used Viridiplantae OrthoDB v10 as a protein homology indicator for our prediction, and RNA-seq spliced alignment was performed with STAR 2.7.6a (default parameter). Gene function annotation was performed by BLASTP ($<1 \times 10^{-5}$) against several known databases (Camacho et al., 2009), including the SwissProt, Kyoto Encyclopedia of Genes and Genomes (KEGG), and NR databases. The domain and gene ontology of the gene models were identified by InterProScan.

Phylogenetic analysis and comparative genomics

Gene sets of sixteen selected plant species (*Xanthoceras sorbifolium*, *Acer yangbiense*, *Litchi chinensis*, *Dimocarpus longan*, *T. vernicifluum* 'Caobachi', *T. vernicifluum* 'Dali', *T. succedaneum* 'Vietnam', *T. succedaneum* 'Japan', *P. vera*, *M. indica*, *A. occidentale*, *S. birrea*, *Citrus sinensis*, *Theobroma cacao*, *Arabidopsis thaliana* and *Vitis vinifera*) were collected for phylogenetic analysis (Table S1). OrthoFinder v2.3.3 (Emms & Kelly, 2019) with default parameters was used to identify orthogroups, generating a total of 261 single-copy gene families. The protein sequences of each selected single-copy gene family were subjected to multiple sequence alignment by MAFFT v7.310 (Katoh & Standley, 2013). Only positions where 50% or more of the sequences had a gap were treated as gap positions in the alignment by an in-house Perl script (https://doi.org/10.6084/m9.figshare.25333939). IQ-TREE2 (Nguyen et al., 2015) was used to infer the maximum likelihood trees with the best-fit evolutionary substitution model predicted by ModelFinder and 500 bootstrap replicates. ASTRAL (Mirarab et al., 2014) was used to summarize the coalescent species tree and the quartet support with default settings.

For gene family expansion and contraction analysis, a phylogenetic tree was constructed by Count (http://www.iro.umontreal.ca/~csuros/gene_content/count.html). Eight representative species (TvD, TvC, TsV, TsJ, *P. vera*, *M. indica*, *S. birrea*, *C. sinensis*, *X. sorbifolium*, and *L. chinensis*) were selected for gene family evolution analysis. OrthoFinder v2.3.3 with default parameters was used to define orthogroups. The numbers of commonly shared gene families and species-specific gene families are displayed in the UpSet plot figure. Key candidate gene detection and evolutionary analysis were performed by functional annotation, BLAST searches and phylogenetic methods (see Methods S1).

Whole-genome duplication identification and genome synteny

To identify ancient whole-genome duplication (WGD) events in Anacardiaceae, the "Wf2" command from the WGD tool (Zwaenepoel & van de Peer, 2019) was used to compute whole-paranome and one-to-one ortholog synonymous substitutions per synonymous site (Ks) distributions from six species (TvD, TvC, TsV, TsJ, *P. vera*, *M. indica*, *S. birrea*, *and A. occidentale*). Tandem duplications were removed from candidate homologous gene pairs by the duplicate_gene_classifier module of the MCScan pipeline with default parameters. The histogram and density plots were drawn by the hist and lines functions of R. In addition, the Ks between the syntenic homologous gene pairs for TvD/TsV, TvD/TsJ, and TsV/TsJ were also calculated using the WGD tool. For genome synteny inference, we used JCVI from the MCScan pipeline (Wang et al., 2012) with default settings. The Ks-based dot plots were generated by "BlockK" of the WGDI (Sun et al., 2022).

Differential expression and coexpression analysis

The gene expression values (FPKM) were calculated using the RSEM package (Li & Dewey, 2011), which was incorporated into trinityrnaseq-2.0.6 (Haas et al., 2013). Furthermore, differentially expressed genes with a false discovery rate ≤0.05 and at least a two-fold change in expression were identified using DESeq2 (Michael I Love 2014): Moderated estimation of fold change and dispersion for RNA-seq data with DESeq2) (see Methods S1). Three coexpression analyses were performed using different transcriptome datasets and programs (the WGCNA [Langfelder & Horvath, 2008] and TO-GCN R packages [Yao-Ming Chang 2019]); see Methods S1 for details on this part of the analysis.

Polyphenols, flavonoids, and lipid detection

Leaf and phloem tissues were collected for analysis of polyphenols (including urushiol) and flavonoids, and fruits were collected for analysis of lipids among *Toxicodendron* species (see Methods S1). The analysis was performed by MetWare (Wuhan, China) following the standard protocol (see details in Methods S1).

Determination of the water and protein contents in developing fruits

Developing fruits from TvD, TsV, and/or TsJ species were collected at different developmental stages. Their water content was determined according to a previously described method (Demir & Ellis, 1992), and their protein content was determined as previously described (Dicumarol, 1975).

AUTHOR CONTRIBUTIONS

CH, SW, and LgL conceived, designed and supervised the project. HLiu, CH, DZ, XZ, PG, XC, JZ, YL, PL, SM, JY, TJ, SL and MR provided resources and materials. SW, YX, LzL and HW generated the draft genomes and performed the annotation. SW, YX, HW, HLiang, XC, LL and SKS analyzed the data. SW, SKS, and YX wrote the manuscript. SW, YX, HLiu, LgL, SKS and CH revised the manuscript. All the authors have read and revised the final version of the manuscript.

ACKNOWLEDGEMENTS

This work was supported by the Yunnan Provincial Expert Workstation (No. 202005AF150020), the Yunnan province Industry and Technology Leading Talent Training Program (No. YUWR-CYJS-2020-018), and the Special Funds for Local Scientific and Technological Development Guided by the Central Government (No. YDZX201953000002845). We thank the Guangdong Provincial Academician Workstation of BGI Synthetic Genomics, BGI-Shenzhen, Guangdong, China. This work is part of the 10KP project and is supported by the China National GenBank.

CONFLICT OF INTEREST STATEMENT

The authors declare no conflicts of interest.

DATA AVAILABILITY STATEMENT

The genome assemblies, annotations and raw data for the three *Toxicodendron* trees in this study were deposited in the CNGB Nucleotide Sequence Archive (CNSA) of the China National GeneBank DataBase (CNGBdb) with accession number CNP0003406 (http://db.cngb.org/search/-project/CNP0003406). All the gene multiple sequence alignments used in the gene tree analyses are available in FigShare (https://doi.org/10.6084/m9.figshare.24197919.v1).

SUPPORTING INFORMATION

Additional Supporting Information may be found in the online version of this article.

Methods S1. Supplemental methods.

Figure S1. Schematic diagram of the plant samplings collected from *Toxicodendron vernicifluum* 'Dali', *Toxicodendron succedaneum* 'Vietnam' and *T. succedaneum* 'Japan'.

Figure S2. The K-mer analyses of three *Toxicodendron* cultivars.

Figure S3. Hi-C contact matrix visualization for pseudochromosomes of three *Toxicodendron* cultivars genome assembly.

Figure S4. Three phylogenetic trees of four *Toxicodendron* cultivars with other 12 species using 261 (top-left), 414 (top-right) single-copy gene families, and 784 low-copy gene families (bottom-left), respectively.

Figure S5. Phylogenetic tree analysis of four *Toxicodendron* cultivars with other selected plants.

Figure S6. Ks distribution of syntenic orthologs from three *Toxicodendron* cultivars, *Anacardium occidentale*, *Mangifera indica*, *Sclerocarya birrea* and *Pistacia vera*.

Figure S7. Ks distribution of syntenic orthologs within three *Toxicodendron* cultivars.

Figure S8. The syntenic plots among *Mangifera indica* (upper), *Anacardium occidentale* (bottom) and *Toxicodendron*, showing their 2:2:1 syntenic depth ratios.

Figure S9. The intergenomic dotplot (left) and corresponding Ks-based dotplot (right) of three *Toxicodendron* cultivars according to the WGDI.

Figure S10. The syntenic plots among three *Toxicodendron* cultivars.

Figure S11. The PAV distributions across the genomes of TvD, TvC, TsV, and TsJ according to pairwise comparisons.

Figure S12. Phylogenetic relationships of the CHS genes of three *Toxicodendron* cultivars with those of other representative taxa.

Figure S13. The five types of lipid concentrations in fruits of the three *Toxicodendron* cultivars from June to September.

Figure S14. Comparison of total lipid concentrations (left), lipid percentages (middle), and unsaturated and saturated LCFA concentrations (right) of fruits among three *Toxicodendron* cultivars from June to September.

Figure S15. Phylogenetic relationships of the FAR genes of three *Toxicodendron* cultivars with those of other representative taxa.

Figure S16. Phylogenetic relationships of the wax-ester biosynthesis-related genes of three *Toxicodendron* cultivars with those of other representative taxa.

Figure S17. Phylogenetic relationships of FAO genes of three *Toxicodendron* cultivars with those of other representative taxa.

Figure S18. The GO enrichment of genes in M1 (Module 1) from the WGCNA of TvD.

Figure S19. Expression profile of genes related to lipid metabolism throughout fruit development, including genes involved in the biosynthetic pathway of fatty acid, wax and Kennedy.

Figure S20. Predicted gene coexpression networks and the connections among TFs and genes involved in biosynthetic pathways of FFAs (blue points), wax (orange points) and Kennedy (pink points).

Figure S21. Comparison of protein and absolute water contents among three *Toxicodendron* fruits from June to September.

Figure S22. Schematics of FFA biosynthesis, wax biosynthesis and Kennedy synthesis in *Toxicodendron*.

Table S1. Species used for plant phylogenetic construction.

Table S2. Statistics of the assemblies of three *Toxicodendron* cultivars.

Table S3. Statistics of chromosome-level assemblies.

Table S4. Completeness evaluation of genes using the Embryophyta_odb10 database.

Table S5. Statistics of repetitive sequences among three *Toxicodendron* cultivars.

Table S6. Statistics of functional annotation.

Table S7. The KEGG enrichment pathways for *Toxicodendron*-specific gene comparison among species within Sapindales from Sapindaceae, Anacardiaceae and Rutaceae.

Table S8. The KEGG enrichment pathways for *Toxicodendron* lineage-expanded genes.

Table S9. Structural variations among the four Toxicodendron cultivars.

Table S10. KEGG enrichment pathways for low-KS genes of three *Toxicodendron* cultivars.

Table S11. The relative content of urushiol (including urushiol I-V and laccol) in the phloem tissue and leaves of TvD, TsV and TsJ.

Table S12. The gene copies of the CHS gene family among three *Toxicodendron* cultivars with other representative species.

Table S13. The CHS gene expression in leaf, fruit, and phloem tissue of three *Toxicodendron* cultivars.

Table S14. The FFA concentration among phloem tissue of TvD, TsV and TsJ.

Table S15. The relative content of chalcone in phloem tissue and leaf of TvD, TsV and TsJ.

Table S16. The lipid concentration among fruits of TvD, TsV and TsJ in different month.

Table S17. The genes in lipid metabolic pathways.

Table S18. The FFA concentration among fruits of TvD, TsV and TsJ in different month.

Table S19. The fruit size of TvD, TsV, and TsJ from June to September.

Table S20. Weighted gene coexpression network analysis of fruits from three *Toxicodendron* cultivars and functional enrichment.

Table S21. The gene expression of lipid metabolism genes in fruits of three *Toxicodendron* cultivars.

Table S22. Time-ordered gene coexpression network analysis for transcription factors and genes involved in lipid metabolism in fruits of three *Toxicodendron* cultivars.

Table S23. The diverse TFs regulating CER in June and July.

Table S24. Comparison of genome statistics between *T. vernicifluum* 'Dali' (TvD) and the published *T. vernicifluum* 'Caobachi'.

Table S25. KEGG enrichment pathways of genes unique to TvD and *T. vernicifluum* 'Caobachi'.

Table S26. The fruit weight (fresh weight and dry weight) of TvD, TsV, and TsJ from June to September.

Table S27. The protein content of the fruits of the TvD, TsV, and TsJ cultivars from June to September.

Table S28. The gene expression of each catalytic step in different tissues of TsJ.

Table S29. The list of abbreviations.

REFERENCES

Ai, W., Liu, Y., Mei, M., Zhang, X., Tan, E., Liu, H. *et al.* (2022) A chromosome-scale genome assembly of the Mongolian oak (*Quercus mongolica*). *Molecular Ecology Resources*, **22**, 2396–2410.

Austin, M.B. & **Noel, J.P.** (2003) The chalcone synthase superfamily of type III polyketide synthases. *Natural Product Reports*, **20**, 79–110.

Aziz, M., Sturtevant, D., Winston, J., Collakova, E., Jelesko, J.G. & **Chapman, K.D.** (2017) MALDI-MS imaging of urushiols in poison ivy stem. *Molecules*, **22**, 711.

Bai, G., Chen, C., Zhao, C., Zhou, T., Li, D., Zhou, T. *et al.* (2022) The chromosome-level genome for *Toxicodendron vernicifluum* provides crucial insights into Anacardiaceae evolution and urushiol biosynthesis. *Iscience*, **25**, 104512.

Bai, G.-Q., Jia, Y., Li, W.-M., Chen, H., Li, B. & **Li, S.-F.** (2018) De novo assembly and analysis of sumac (*Toxicodendron vernicifluum* (stokes) FA Barkley) transcriptomes provides insights into the biosynthesis of urushiol. *Molecular Biology*, **52**, 660–667.

Beaman, J.H. (1986) Allergenic Asian Anacardiaceae. *Clinics in Dermatology*, **4**, 191–203.

Bemelmans, W., Muskiet, F., Feskens, E., de Vries, J., Broer, J., May, J. *et al.* (2000) Associations of alpha-linolenic acid and linoleic acid with risk factors for coronary heart disease. *European Journal of Clinical Nutrition*, **54**, 865–871.

Bourdenx, B., Bernard, A., Domergue, F., Pascal, S., Léger, A., Roby, D. *et al.* (2011) Overexpression of *Arabidopsis* ECERIFERUM1 promotes wax very-long-chain alkane biosynthesis and influences plant response to biotic and abiotic stresses. *Plant Physiology*, **156**, 29–45.

Camacho, C., Coulouris, G., Avagyan, V., Ma, N., Papadopoulos, J., Bealer, K. *et al.* (2009) BLAST+: architecture and applications. *BMC Bioinformatics*, **10**, 1–9.

Chen, X., Wang, P., Wei, M., Lin, X., Gu, M., Fang, W. *et al.* (2022) Lipidomics analysis unravels changes from flavor precursors in different processing treatments of purple-leaf tea. *Journal of the Science of Food and Agriculture*, **102**, 3730–3741.

Cheng, Q., Liu, H.-T., Bombelli, P., Smith, A. & **Slabas, A.R.** (2004) Functional identification of AtFao3, a membrane bound long chain alcohol oxidase in *Arabidopsis thaliana*. *FEBS Letters*, **574**, 62–68.

Cho, J.-Y., Park, K.Y., Kim, S.-J., Oh, S. & **Moon, J.-H.** (2015) Antimicrobial activity of the synthesized non-allergenic urushiol derivatives. *Bioscience, Biotechnology, and Biochemistry*, **79**, 1915–1918.

Czemmel, S., Heppel, S.C. & **Bogs, J.** (2012) R2R3 MYB transcription factors: key regulators of the flavonoid biosynthetic pathway in grapevine. *Protoplasma*, **249**, 109–118.

Dawson, C.R. & **Kurtz, A.P.** (1971) Synthesis of compounds structurally related to poison ivy urushiol. 4. 3-(1-alkyl) alkylcatechols of varying side-chain shape and flexibility. *Journal of Medicinal Chemistry*, **14**, 733–737.

Demir, I. & **Ellis, R.** (1992) Changes in seed quality during seed development and maturation in tomato. *Seed Science Research*, **2**, 81–87.

Dicumarol, B.S. (1975) Errata and emendations, official methods of analysis, AOAC. *Amino Acids*, **16**, A01.

Doan, T.T., Carlsson, A.S., Hamberg, M., Bülow, L., Stymne, S. & **Olsson, P.** (2009) Functional expression of five Arabidopsis fatty acyl-CoA reductase genes in *Escherichia coli*. *Journal of Plant Physiology*, **166**, 787–796.

Dobin, A., Davis, C.A., Schlesinger, F., Drenkow, J., Zaleski, C., Jha, S. *et al.* (2013) STAR: ultrafast universal RNA-seq aligner. *Bioinformatics*, **29**, 15–21.

Eastmond, P.J. (2006) SUGAR-DEPENDENT1 encodes a patatin domain triacylglycerol lipase that initiates storage oil breakdown in germinating *Arabidopsis* seeds. *The Plant Cell*, **18**, 665–675.

Edgar, R.C. & **Myers, E.W.** (2005) PILER: identification and classification of genomic repeats. *Bioinformatics*, **21**, i152–i158.

El-Kouhen, K., Blangy, S., Ortiz, E., Gardies, A.-M., Ferté, N. & **Arondel, V.** (2005) Identification and characterization of a triacylglycerol lipase in *Arabidopsis* homologous to mammalian acid lipases. *FEBS Letters*, **579**, 6067–6073.

Emms, D.M. & **Kelly, S.** (2019) OrthoFinder: phylogenetic orthology inference for comparative genomics. *Genome Biology*, **20**, 1–14.

Ferreira, C.D.S., **Piedade, M.T.F.**, **Tiné, M.A.S.**, **Rossatto, D.R.**, **Parolin, P.** & **Buckeridge, M.S.** (2009) The role of carbohydrates in seed germination and seedling establishment of *Himatanthus sucuuba*, an Amazonian tree with populations adapted to flooded and non-flooded conditions. *Annals of Botany*, **104**, 1111–1119.

Frankel, E. (1991) *Poison ivy, poison oak, poison sumac, and their relatives*. Kennebunk: Boxwood Press.

Geissman, T. (1963) The biosynthesis of phenolic plant products. In: Peter, B. (Ed.)*Biogenesis of natural compounds*. Amsterdam: Elsevier, pp. 743–799.

Gladman, A.C. (2006) Toxicodendron dermatitis: poison ivy, oak, and sumac. *Wilderness & Environmental Medicine*, **17**, 120–128.

Gu, C., **Guo, Z.-H.**, **Hao, P.-P.**, **Wang, G.-M.**, **Jin, Z.-M.** & **Zhang, S.-L.** (2017) Multiple regulatory roles of AP2/ERF transcription factor in angiosperm. *Botanical Studies*, **58**, 1–8.

Guijas, C., **Montenegro-Burke, J.R.**, **Domingo-Almenara, X.**, **Palermo, A.**, **Warth, B.**, **Hermann, G.** ***et al.*** (2018) METLIN: a technology platform for identifying knowns and unknowns. *Analytical Chemistry*, **90**, 3156–3164.

Haas, B.J., **Papanicolaou, A.**, **Yassour, M.**, **Grabherr, M.**, **Blood, P.D.**, **Bowden, J.** ***et al.*** (2013) *De novo* transcript sequence reconstruction from RNA-seq using the Trinity platform for reference generation and analysis. *Nature Protocols*, **8**, 1494–1512.

Hoff, K.J., **Lange, S.**, **Lomsadze, A.**, **Borodovsky, M.** & **Stanke, M.** (2016) BRAKER1: unsupervised RNA-Seq-based genome annotation with GeneMark-ET and AUGUSTUS. *Bioinformatics*, **32**, 767–769.

Hu, G., **Feng, J.**, **Xiang, X.**, **Wang, J.**, **Salojärvi, J.**, **Liu, C.** ***et al.*** (2022) Two divergent haplotypes from a highly heterozygous lychee genome suggest independent domestication events for early and late-maturing cultivars. *Nature Genetics*, **54**, 73–83.

Kambhampati, S., **Aznar-Moreno, J.A.**, **Bailey, S.R.**, **Arp, J.J.**, **Chu, K.L.**, **Bilyeu, K.D.** ***et al.*** (2021) Temporal changes in metabolism late in seed development affect biomass composition. *Plant Physiology*, **186**, 874–890.

Kamiya, Y., **Saito, W.** & **Miyakoshi, T.** (2002) Synthesis and identification of laccol components from *Rhus succedanea* lacquer sap. *Journal of Oleo Science*, **51**, 473–483.

Katoh, K. & **Standley, D.M.** (2013) MAFFT multiple sequence alignment software version 7: improvements in performance and usability. *Molecular Biology and Evolution*, **30**, 772–780.

Kent, W.J. (2002) BLAT—the BLAST-like alignment tool. *Genome Research*, **12**, 656–664.

Langfelder, P. & **Horvath, S.** (2008) WGCNA: an R package for weighted correlation network analysis. *BMC Bioinformatics*, **9**, 1–13.

Li, B. & **Dewey, C.N.** (2011) RSEM: accurate transcript quantification from RNA-Seq data with or without a reference genome. *BMC Bioinformatics*, **12**, 1–16.

Li, D., **Li, K.** & **Fang, J.** (2022) Research progress on modification and application of raw lacquer. *ChemistrySelect*, **7**, e202200943.

Li, S., **Huang, H.**, **Ma, X.**, **Hu, Z.**, **Li, J.** & **Yin, H.** (2022) Characterizations of MYB transcription factors in *Camellia oleifera* reveal the key regulators involved in oil biosynthesis. *Horticulturae*, **8**, 742.

Li, S., **Wang, X.**, **He, S.**, **Li, J.**, **Huang, Q.**, **Imaizumi, T.** ***et al.*** (2016) CFLAP1 and CFLAP2 are two bHLH transcription factors participating in synergistic regulation of AtCFL1-mediated cuticle development in *Arabidopsis*. *PLoS Genetics*, **12**, e1005744.

Li, W., **Bai, G.**, **Chen, H.**, **Li, B.** & **Li, S.** (2017) Advance in research on genetic diversity of *Toxicodendron vernicifluum* (in Chinese). *Shananxi Forest Science and Technology*, **104**, 97–100.

Lin, Y., **Min, J.**, **Lai, R.**, **Wu, Z.**, **Chen, Y.**, **Yu, L.** ***et al.*** (2017) Genome-wide sequencing of longan (*Dimocarpus longan* Lour.) provides insights into molecular basis of its polyphenol-rich characteristics. *GigaScience*, **6**, gix023.

Liu, L., **Cai, F.**, **Lu, Y.**, **Xie, Y.**, **Li, H.** & **Long, C.** (2022) Comparative lipidomic and metabolomic analyses reveal the mystery of lacquer oil from *Toxicodendron vernicifluum* for the treatment of "Yuezi" disease in Nujiang, China: from anti-inflammation and anti-postpartum depression perspective. *Frontiers in Pharmacology*, **13**, 914951.

Liu, Y.-F., **Li, Q.-T.**, **Lu, X.**, **Song, Q.-X.**, **Lam, S.-M.**, **Zhang, W.-K.** ***et al.*** (2014) Soybean GmMYB73 promotes lipid accumulation in transgenic plants. *BMC Plant Biology*, **14**, 1–16.

Lou, H., **Song, L.**, **Li, X.**, **Zi, H.**, **Chen, W.**, **Gao, Y.** ***et al.*** (2023) The *Torreya grandis* genome illuminates the origin and evolution of gymnosperm-specific sciadonic acid biosynthesis. *Nature Communications*, **14**, 1315.

Majima, R. (1922) Über den Hauptbestandteil des Japan-Lacks, IX. Mitteilung: Chemische Untersuchung der verschiedenen natürlichen Lackarten, die dem Japan-Lack nahe verwandt sind. *Berichte der deutschen chemischen Gesellschaft (A and B Series)*, **55**, 191–214.

Majima, R. & **Chō, S.** (1907) Ueber einen hauptbestandteil des japanischen lackes. *Berichte der Deutschen Chemischen Gesellschaft*, **40**, 4390–4393.

Mirarab, S., **Reaz, R.**, **Bayzid, M.S.**, **Zimmermann, T.**, **Swenson, M.S.** & **Warnow, T.** (2014) ASTRAL: genome-scale coalescent-based species tree estimation. *Bioinformatics*, **30**, i541–i548.

Miyamoto, T., **Tobimatsu, Y.** & **Umezawa, T.** (2020) MYB-mediated regulation of lignin biosynthesis in grasses. *Current Plant Biology*, **24**, 100174.

Nguyen, L.-T., **Schmidt, H.A.**, **Von Haeseler, A.** & **Minh, B.Q.** (2015) IQ-TREE: a fast and effective stochastic algorithm for estimating maximum-likelihood phylogenies. *Molecular Biology and Evolution*, **32**, 268–274.

Nie, Z.L., **Sun, H.**, **Meng, Y.** & **Wen, J.** (2009) Phylogenetic analysis of *Toxicodendron* (Anacardiaceae) and its biogeographic implications on the evolution of north temperate and tropical intercontinental disjunctions. *Journal of Systematics and Evolution*, **47**, 416–430.

Niimura, N., **Miyakoshi, T.**, **Onodera, J.** & **Higuchi, T.** (1996) Characterization of *Rhus vernicifera* and *Rhus succedanea* lacquer films and their pyrolysis mechanisms studied using two-stage pyrolysis-gas chromatography/mass spectrometry. *Journal of Analytical and Applied Pyrolysis*, **37**, 199–209.

Oshima, R., **Yamauchi, Y.**, **Watanabe, C.** & **Kumanotani, J.** (1985) Enzymic oxidative coupling of urushiol in sap of the lac tree, Rhus vernicifera. *The Journal of Organic Chemistry*, **50**, 2613–2621.

Ou, S. & **Jiang, N.** (2018) LTR_retriever: a highly accurate and sensitive program for identification of long terminal repeat retrotransposons. *Plant Physiology*, **176**, 1410–1422.

Patwari, P., **Salewski, V.**, **Gutbrod, K.**, **Kreszies, T.**, **Dresen-Scholz, B.**, **Peisker, H.** ***et al.*** (2019) Surface wax esters contribute to drought tolerance in *Arabidopsis*. *The Plant Journal*, **98**, 727–744.

Qin, M., **Mitchell, J.D.** & **Vogl, O.** (1996) Oriental lacquer. 10. The South East Asian lacquer. *Journal of Macromolecular Science, Part A: Pure and Applied Chemistry*, **33**, 1791–1803.

Rajavel, A., **Klees, S.**, **Schlüter, J.-S.**, **Bertram, H.**, **Lu, K.**, **Schmitt, A.O.** ***et al.*** (2021) Unravelling the complex interplay of transcription factors orchestrating seed oil content in *Brassica napus* L. *International Journal of Molecular Sciences*, **22**, 1033.

Sahu, S.K., **Thangaraj, M.** & **Kathiresan, K.** (2012) DNA extraction protocol for plants with high levels of secondary metabolites and polysaccharides without using liquid nitrogen and phenol. *International Scholarly Research Notices*, **2012**, 205049.

Saravanakumar, K., **Chelliah, R.**, **Hu, X.**, **Oh, D.-H.**, **Kathiresan, K.** & **Wang, M.-H.** (2019) Antioxidant, anti-lung cancer, and anti-bacterial activities of *Toxicodendron vernicifluum*. *Biomolecules*, **9**, 127.

Seo, P.J., **Lee, S.B.**, **Suh, M.C.**, **Park, M.-J.**, **Go, Y.S.** & **Park, C.-M.** (2011) The MYB96 transcription factor regulates cuticular wax biosynthesis under drought conditions in *Arabidopsis*. *The Plant Cell*, **23**, 1138–1152.

Simão, F.A., **Waterhouse, R.M.**, **Ioannidis, P.**, **Kriventseva, E.V.** & **Zdobnov, E.M.** (2015) BUSCO: assessing genome assembly and annotation completeness with single-copy orthologs. *Bioinformatics*, **31**, 3210–3212.

Snyder, D.M. (1989) An overview of oriental lacquer: art and chemistry of the original high-tech coating. *Journal of Chemical Education*, **66**, 977.

Suk, K.T., **Baik, S.K.**, **Kim, H.S.**, **Park, S.M.**, **Paeng, K.J.**, **Uh, Y.** ***et al.*** (2011) Antibacterial effects of the urushiol component in the sap of the lacquer tree (*Rhus verniciflua* Stokes) on *Helicobacter pylori*. *Helicobacter*, **16**, 434–443.

Sun, P., **Jiao, B.**, **Yang, Y.**, **Shan, L.**, **Li, T.**, **Li, X.** ***et al.*** (2022) WGDI: a user-friendly toolkit for evolutionary analyses of whole-genome duplications and ancestral karyotypes. *Molecular Plant*, **15**, 1841–1851.

Sunthankar, S. & **Dawson, C.R.** (1954) The structural identification of the olefinic components of Japanese lac urushiol. *Journal of the American Chemical Society*, **76**, 5070–5074.

Symes, W. & **Dawson, C.R.** (1953) Separation and structural determination of the olefinic components of poison ivy urushiol, cardanol and cardol. *Nature*, **171**, 841–842.

Tong, J., **Yang, S.**, **Chen, F.**, **Chen, Z.**, **Zhai, J.** & **Xu, D.** (2019) Research progress on Toxicodendron succedaneum (in Chinese). *Hubei Agricultural Sciences*, **58**, 16–20.

Tsujimoto, M. (1935) On the fatty acids of Japan wax. *Bulletin of the Chemical Society of Japan*, **10**, 212–219.

Verdaguer, R., **Soler, M.**, **Serra, O.**, **Garrote, A.**, **Fernández, S.**, **Company-Arumí, D.** ***et al.*** (2016) Silencing of the potato StNAC103 gene enhances the accumulation of suberin polyester and associated wax in tuber skin. *Journal of Experimental Botany*, **67**, 5415–5427.

Vurture, G.W., **Sedlazeck, F.J.**, **Nattestad, M.**, **Underwood, C.J.**, **Fang, H.**, **Gurtowski, J.** ***et al.*** (2017) GenomeScope: fast reference-free genome profiling from short reads. *Bioinformatics*, **33**, 2202–2204.

Walker, B.J., **Abeel, T.**, **Shea, T.**, **Priest, M.**, **Abouelliel, A.**, **Sakthikumar, S.** ***et al.*** (2014) Pilon: an integrated tool for comprehensive microbial variant detection and genome assembly improvement. *PLoS One*, **9**, e112963.

Wang, P., **Luo, Y.**, **Huang, J.**, **Gao, S.**, **Zhu, G.**, **Dang, Z.** ***et al.*** (2020) The genome evolution and domestication of tropical fruit mango. *Genome Biology*, **21**, 1–17.

Wang, Y., **Tang, H.**, **DeBarry, J.D.**, **Tan, X.**, **Li, J.**, **Wang, X.** ***et al.*** (2012) MCScanX: a toolkit for detection and evolutionary analysis of gene synteny and collinearity. *Nucleic Acids Research*, **40**, e49.

Wei, S., **Fu, S.** & **Hu, Z.** (2009) Variation of urushiol content in raw lacquer and the bark structure of *Toxicodendron vernicifluum* in different seasons and their correlation. *Scientia Silvae Sinica*, **45**, 67–73.

Weisberg, A.J. (2014) *Investigations into the molecular evolution of plant terpene, alkaloid, and urushiol biosynthetic enzymes*. Blacksburg: Virginia Tech.

Wu, G.-Z. & **Xue, H.-W.** (2010) *Arabidopsis* β-ketoacyl-[acyl carrier protein] synthase I is crucial for fatty acid synthesis and plays a role in chloroplast division and embryo development. *The Plant Cell*, **22**, 3726–3744.

Xie, T., **Zheng, J.-F.**, **Liu, S.**, **Peng, C.**, **Zhou, Y.-M.**, **Yang, Q.-Y.** ***et al.*** (2015) *De novo* plant genome assembly based on chromatin interactions: a case study of *Arabidopsis thaliana*. *Molecular Plant*, **8**, 489–492.

Xie, Y., **Zhang, J.**, **Liu, W.**, **Xie, N.**, **Feng, F.** & **Qu, W.** (2016) New urushiols with platelet aggregation inhibitory activities from resin of *Toxicodendron vernicifluum*. *Fitoterapia*, **112**, 38–44.

Xu, W., **Li, F.**, **Ling, L.** & **Liu, A.** (2013) Genome-wide survey and expression profiles of the AP2/ERF family in castor bean (*Ricinus communis* L.). *BMC Genomics*, **14**, 1–15.

Xu, Z. & **Wang, H.** (2007) LTR_FINDER: an efficient tool for the prediction of full-length LTR retrotransposons. *Nucleic Acids Research*, **35**, W265–W268.

Yamauchi, Y., **Oshima, R.** & **Kumanotani, J.** (1980) Separation of Japanese lac urushiol diacetate on silver nitrate-coated silica gel columns by high-performance liquid chromatography. *Journal of Chromatography A*, **198**, 49–56.

Yu, X. (2014) Typical characteristics and application of Vietnam lacquer (in Chinese). *Journal of Chinese Lacquer*, **33**, 31–33.

Zhang, X., **Chen, S.**, **Shi, L.**, **Gong, D.**, **Zhang, S.**, **Zhao, Q.** ***et al.*** (2021) Haplotype-resolved genome assembly provides insights into evolutionary history of the tea plant *Camellia sinensis*. *Nature Genetics*, **53**, 1250–1259.

Zhao, M. (2021) Research progress on the resin canal and raw lacquer synthesis of *Toxicodendron vernicifluum* (Stokes) FA Barkley. In: Ramawat, K.G., Ekiert, H.M. & Goyal, S. (Eds.) *Plant cell and tissue differentiation and secondary metabolites: fundamentals and applications*. Berlin: Springer, pp. 145–165.

Zhao, W., **Zhu, L.**, **Srinivasan, S.**, **Damodaran, C.** & **Rohr, J.** (2009) Identification of urushiols as the major active principle of the Siddha herbal medicine Semecarpus Lehyam: anti-tumor agents for the treatment of breast cancer. *Pharmaceutical Biology*, **47**, 886–893.

Zheng, J., **Meinhardt, L.W.**, **Goenaga, R.**, **Matsumoto, T.**, **Zhang, D.** & **Yin, Y.** (2022) The chromosome-level rambutan genome reveals a significant role of segmental duplication in the expansion of resistance genes. *Horticulture Research*, **9**, uhac014.

Zwaenepoel, A. & **van de Peer, Y.** (2019) wgd—simple command line tools for the analysis of ancient whole-genome duplications. *Bioinformatics*, **35**, 2153–2155.